Viscoelastic Structural Properties of Human Ribs in a Simulated Frontal Impact

Yun-Seok Kang, Kevin Moorhouse, John H. Bolte IV, Jason Stammen, Amanda M. Agnew

Abstract The objective of this study was to develop models for exploring viscoelastic structural properties of human ribs in a simulated frontal impact scenario. Three hundred eighty-one ribs from 207 individuals were dynamically tested to simulate anterior-posterior bending in a frontal impact scenario. Two models, a second order mass-damper-spring model and a piecewise model with mass-damper-spring were proposed to replicate rib reaction force using acceleration, velocity, and displacement data collected during testing. The piecewise model was composed of two piecewise components: one for the initial loading phase and the other for the subsequent loading phase. An optimization technique was used to determine parameters of the proposed models by maximizing the coefficient of determination between the proposed models and actual rib responses. Results show the piecewise model successfully mimicked the rib force data (332 of 381 ribs had R-sq ≥ 0.99), while the mass-damper-spring model exhibited less accurate responses (129 of 381 ribs had R-sq ≥ 0.99). Based on a lack of viscoelastic structural properties of human ribs in the literature, these data should help researchers better understand rib structural behavior in a frontal impact scenario.

Keywords Human thorax, human rib, rib damping, structural properties, viscoelasticity.

I. INTRODUCTION

Thoracic injury is associated with high rates of morbidity and mortality, especially in the form of rib fractures in motor vehicle crashes, and these rates have not been declining [1]. Rib fractures are the most predominate thorax injury and have received considerable attention [2-7]. Experimental approaches using post-mortem human subjects (PMHSs) such as full sled tests [8-10], hub impact tests [11-13], and bench top tests [14-15] have been used to investigate thoracic biomechanical responses and injuries, e.g., rib fractures. Although these studies successfully provided gross thoracic response and identified rib fractures, biomechanical behavior of thoracic components, such as the ribs, should also be investigated to understand relevant biomechanical parameters and predictors of rib fractures.

Whole rib experiments have been performed to better understand structural properties and responses in various loading conditions [16-19]. Structural properties of the ribs, such as peak force, peak displacement, stiffness, and energy have been deemed critical parameters that represented mechanical behaviors of human ribs. These structural properties have also been utilized to seek meaningful relationships with several different factors, such as rib overall geometry, rib section properties, material content (e.g., ash density, mineral linear density), and material properties [16-19]. However, these simplified structural properties do not adequately represent the entire structural response from the beginning of impact to the time of rib fracture. The complete structural responses of human ribs exhibit both elastic and plastic characteristics, with the plastic characteristic often most evident in pediatric and young adults [17]. More importantly, fractures usually occur in the plastic region of rib structural response curves. Due to these plastic characteristics of their structural response, ribs do not behave as linear springs. Moreover, determining stiffness often requires subjectivity in defining the elastic region [17-18]. Therefore, analytical models should be investigated to determine structural properties that can represent both elastic and plastic characteristics of rib structural responses without subjectivity.

Similar, but more complicated, structural responses than those of isolated ribs have been observed in frontal thoracic impact tests [11-12][15]. Analytical models producing viscoelastic structural properties using multiple mass-spring-damper connections were developed and were able to successfully characterize thoracic structural

Y. Kang (e-mail: yunseok.kang@osumc.edu, tel: +1 614 366 7584), PhD is an Assistant Professor, J. Bolte, PhD, and A. Agnew, PhD at the Injury Biomechanics Research Center at The Ohio State University in Columbus, OH, USA, J. Stammen, PhD and K. Moorhouse, PhD are at the National Highway Traffic Safety Administration (NHTSA), USA.

responses for both elastic and plastic regions in blunt impacts [20-22]. Despite this success, the structural viscosity (e.g., damping) has not previously been considered in a scaling technique for the thorax [23]. Adding a damping term into the scaling equation could possibly enhance current scaling techniques. However, PMHS thoracic impact data are limited, making it difficult to develop and validate a new scaling technique for the thorax that is applicable to all demographics (e.g., pediatric to adults). Therefore, it is important to bridge thoracic viscoelastic structural properties with rib viscoelastic structural properties, since a comprehensive rib sample of all ages were previously tested [17] and are used in this study.

The objective of this study was to explore analytical models for determining viscoelastic structural properties of human ribs in a simulated frontal impact scenario. This study intended to serve as a proof of concept for the use of analytical models in determining rib viscoelastic structural properties from a well-controlled experimental set-up.

II. METHODS

Materials and Experimental Set-up

Three hundred eighty-one ribs from 207 post-mortem human subjects (282 male, 99 female) ranging in age from 6 to 99 years were dynamically tested in anterior-posterior bending to mimic a frontal impact scenario. All specimens were ethically obtained from the body donor program at The Ohio State University. Ethics protocols related to this study were reviewed by appropriate research ethics advisory committees. A custom experimental fixture with a 54 kg pendulum mass was utilized to create input velocities (1 and 2 m/s) and energy to cause rib failure during the event (Fig. 1) [17]. Although various instrumentation was used and installed on the fixture and rib, only instrumentation relevant to this study is discussed here. A six-axis load cell (Humanetics, CRABI neck load cell, IF-954, Plymouth, MI, USA) was installed to measure reaction loads at the end opposite to the impact location. An accelerometer (Endevco model 7264C-2K, Endevco, San Juan Capistrano, CA, USA) and a string potentiometer (AMETEK, Rayelco P-20A, Berwyn, PA, USA) were utilized to quantify acceleration, velocity, and displacement of the ribs. The sternal end of the rib was attached to the moving cart, while the vertebral end of the rib was attached to the stationary fixture. In this way, the sternal rib end was translated towards the vertebral end (anterior to posterior) via the pendulum (Fig.1). Further detailed information on instrumentation, the experimental fixture, and rib preparation can be found in [17].

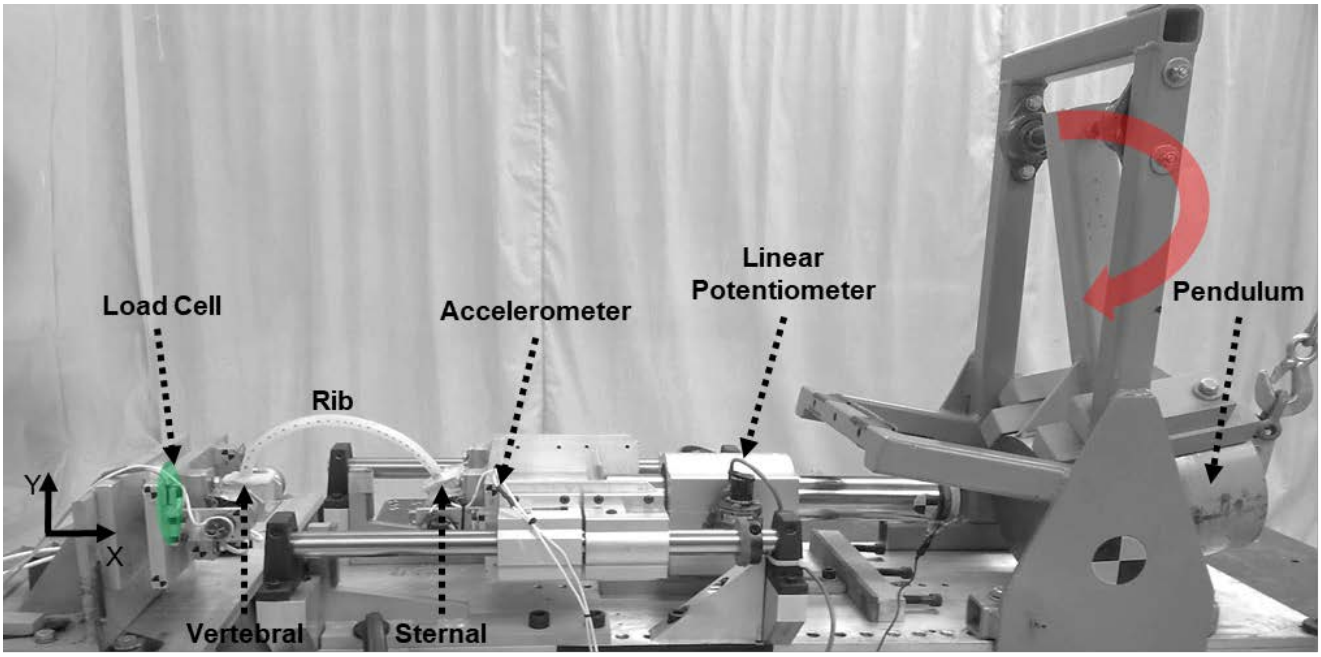

Fig.1. General experimental set-up and instrumentation.

Data Processing and Proposed Models

Force, acceleration, and displacement data were collected using a DTS G5 data acquisition system (Diversified Technical System, Inc., Seal Beach, CA, USA) with a sampling rate of 20,000 Hz. Time-history data for the force, acceleration, and displacement were first truncated at the time of fracture. These data were then filtered at 300 Hz using a 4th order Butterworth phase-less filter in MATLAB (Mathworks, Natick, MA, USA) prior to using analytical models. A custom MATLAB code was developed to create two viscoelastic models with mass, damping and stiffness as shown in Eqs.(1) and (2). These models were proposed in order to replicate rib reaction force in the primary axis of loading, i.e., X-axis, by using acceleration, velocity, and displacement data collected during testing. The first model (referred to as MCK model, hereafter) was a 2nd order mass-damper-spring model (M_1-C_1-K_1) as in Eq.(1), while the second model (referred to as PW model, hereafter) was a piecewise model composed of one mass coefficient (M_2), two damping coefficients (C_{21} and C_{22}), two stiffness coefficients (K_{21} and K_{22}), and a transition point (t_{tp}) as in Eq.(2). The MCK model was attempted under the assumption that the bone can be characterized by a linear spring, while the bone marrow can be represented by a damper with an effective mass (e.g., impacting portion of the rib mass). The PW model was attempted since two distinct behaviors (elastic and plastic) were observed in force time histories from the rib tests. The PW model was composed of two piecewise components: one for the initial loading phase (ILP) and the other for the subsequent loading phase (SLP) as shown in Eq.(2). Since the main acceleration responses occurred in the ILP, no mass coefficient was used in the SLP. For both models, the spring and damper was considered a parallel connection under the assumption that the stiffness terms were influenced by hard tissue (i.e., bone), while the damping terms were affected by bone marrow. An optimization technique in conjunction with the *lsqcurvefit* command in MATLAB was employed to determine optimal design variables, e.g., M_i, C_{ij}, and K_{ij}, in both proposed models by maximizing a pre-defined objective function: the coefficient of determination, R-square (R-sq), between force calculated from the proposed viscoelastic model and force from the rib test (Eq.3). Inequality constraint equations were applied to the optimization method, in order to determine positive values for the design variables (M_i, C_{ij}, and K_{ij}) (Eq.3).

$$F_1(\mathrm{t}) = M_1 a(t) + C_1 v(t) + K_1 d(t) \tag{1}$$

$$F_2(\mathrm{t}) = \begin{matrix} M_2 a(t) + C_{21} v(t) + K_{21} d(t), & t_{tp} < transition\ point\colon\ ILP \\ C_{22} v(t) + K_{22} d(t), & t_{tp} \geq transition\ point\colon SLP \end{matrix} \tag{2}$$

where, $a(t)$: acceleration time history measured from the accelerometer
$v(t)$: velocity time history from numerical integration of the accelerometer data
$d(t)$: displacement time history measured from the string potentiometer

$$\begin{aligned} &\text{Objective function: } Maximize\left(1 - \frac{\sum_0^{t_{fx}} (F_{exp}(t) - F_i(t))^2}{\sum_0^{t_{fx}} (F_{exp}(t) - \overline{F_{exp}})^2}\right) \\ &\text{Design variables: } M_1, C_1, \text{ and } K_1 \text{ for the MCK model} \\ &\qquad\qquad M_2, C_{21}, K_{21}, C_{22}, K_{22}, \text{ and } t_{tp} \text{ for the PW model} \\ &\text{Inequality constraint equations: all design variables} \geq 0 \end{aligned} \tag{3}$$

where, $F_{exp}(\mathrm{t})$: force time history measured from the load cell
$F_i(\mathrm{t})$: calculated force time history from MCK model (Eq. 1) and PW model (Eq. 2)
$\overline{F_{exp}}$: average experimental force data
t_{fx}: time of fracture

Paired t-tests were utilized to explore all differences in design variables, e.g., M, C, and K, between the two models. An alpha (α) value of 0.005 was used to determine statistical significance.

Different Demographics

To better understand the physical significance of each coefficient determined from the model fit to experimental data, an analysis was attempted using different demographics. Model optimization results were separated into three groups: pediatric (0-21 years), adult male (22+ years), and adult female (22+ years). A one-way analysis of variance (ANOVA) was performed to test for significant differences between group means with Tukey's post-hoc test to identify specific differences between groups.

III. RESULTS

The proposed PW model successfully mimicked the rib force time histories with an average R-sq of 0.993 (minimum of 0.778 and maximum of 0.999) and an average root mean square error (RMSE) of 2.2, while the MCK model exhibited less accurate predictive responses than the PW model with an average R-sq of 0.965 (minimum of 0.603 and maximum of 0.999) and an average RMSE of 6.1 as shown in Table I. Fig.2 shows frequency of R-sq values obtained from both models. Three hundred twenty-two ribs (84.5%) had greater than 0.99 R-sq in the PW model, while only 129 ribs (33.9%) had an R-sq greater than 0.99 in the MCK model (Fig.2). Therefore, the PW model was shown to be able to replicate experimental rib responses better than the MCK model. Exemplar acceleration, velocity, displacement, and force time (F-T) histories from rib tests are provided in Fig.A1, while exemplar model outcomes determined from the same rib tests are shown in Fig.A2. Even with different magnitudes and shapes of the F-T curves as shown in Fig.A2, the PW model was able to mimic the experimental rib F-T responses well.

Average effective mass, damping, and stiffness for the MCK model were 1.2 grams, 13.7 N-s/m, and 2.1 N/mm, respectively (Table I). To break it down further, the average effective mass, damping, and stiffness for a sub-model in the ILP were 4.8 grams, 5.6 N-s/m, and 3.0 N/mm, while effective damping and stiffness for a sub-model in the SLP were 34.3 N-s/m and 1.3 N/mm, respectively. The mass, damping and stiffness coefficients determined from the MCK model were significantly different than those from the PW model ($p<0.001$). When damping and stiffness coefficients from the sub-model in ILP were compared to those from the sub-model in SLP, they were also significantly different ($p<0.001$).

TABLE I
OPTIMIZATION RESULTS FROM TWO PROPOSED MODELS

Mean (SD)	n	M_1	C_1	K_1	R-sq1	RMSE1	M_2	C_{21}	C_{22}	K_{21}	K_{22}	R-sq2	RMSE2
Total	381	1.2 (3.1)	13.7 (11.0)	2.1 (1.2)	0.965 (0.049)	6.1 (4.7)	4.8 (6.1)	5.6 (3.9)	34.3 (28.4)	3.0 (1.6)	1.3 (1.0)	0.993 (0.019)	2.2 (1.9)

Units: M (gram), C (N-s/m), K (N/mm)

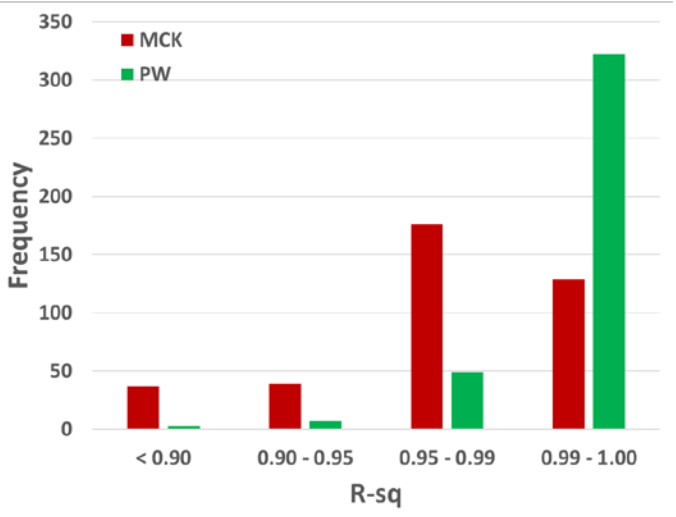

Fig.2. Frequency of R-square results from MCK and PW models.

Since the PW model successfully replicated elastic and plastic responses, results from the PW model were compared for different demographics. For the effective mass, M_2, no significant differences between age groups were ascertained (p = 0.01, Fig.B1). When effective stiffness and damping coefficients were compared, the means between age groups were significantly different. For effective stiffness, the adult male ribs were significantly greater than the pediatric (p=0.003 for K_{21}, p<0.001 for K_{22}) and the adult female ribs (p<0.001 for both K_{21} and K_{22}). Interval plots for the effective stiffness differences are shown in Fig.B2 and B3. Importantly, the pediatric effective stiffness (K_{21}) was significantly larger than the adult female effective stiffness in the ILP (p= 0.002), which is consistent with previous findings [21]. For effective damping, pediatric ribs had significantly higher C_{21} values than adult male (p=0.002) and adult female (p=0.002) (Fig.B4). Similarly, pediatric ribs also exhibited larger C_{22} than adult female (p<0.001) and adult male (p=0.024), and the adult male ribs had significantly larger C_{22} than the adult female (p=0.003) as well (Fig.B5). These results indicate that effective rib viscosity plays an important role in pediatric rib responses, specifically, with more significant plastic responses than in adults [17]. The plastic responses of pediatric rib structural behavior could be replicated by large effective damping coefficients (e.g., C_{21} and C_{22}) in the PW model (Table II).

TABLE II
OPTIMIZATION RESULTS FROM PW MODELS

Mean (SD)	n	M_2	C_{21}	C_{22}	K_{21}	K_{22}	R-sq2	RMSE2
Adult Male	236	4.1 (5.6)	5.4 (3.8)	35.3 (27.9)	3.4 (1.6)	1.6 (1.0)	0.994 (0.014)	2.2 (1.9)
Adult Female	87	6.3 (6.3)	5.1 (2.6)	23.8 (20.0)	1.9 (1.4)	0.9 (0.7)	0.993 (0.014)	1.5 (1.2)
Pediatric	58	5.3 (7.1)	7.1 (5.4)	45.9 (35.2)	2.7 (1.3)	0.7 (0.7)	0.986 (0.032)	3.3 (3.5)

Units: M (gram), C (N-s/m), K (N/mm)

IV. DISCUSSION

Two viscoelastic models were explored in this study. Based on the results from this study, the stand-alone 2nd order MCK analytical model was not able to accurately mimic the experimental F-T responses. Using the MCK model, only 33.9% of the ribs had successful replication (R-sq >0.99) of the experimental F-T responses (average R-sq of 0.965 $\pm$ 0.049), whereas the PW model demonstrated successful replication of the experimental F-T responses for 87.1% of the ribs (average R-sq of 0.993 $\pm$ 0.019). The PW model was proposed in order to accommodate both elastic and plastic regions by determining transition points (e.g., t_{tp} in the optimization). Since M_1, C_1, and K_1 coefficients determined from the MCK model were statistically different from those obtained from the PW model, the MCK model may not be appropriate for future use. The MCK model tended to show better fit to the experimental F-T responses only with small or absent non-linear plastic regions (Fig. A2-c and –h), which is a major drawback of the MCK model. However, the main purpose of including the MCK model in this study was to investigate if such a simple model could characterize structural behavior of whole ribs. In order to check if adding nonlinearity terms for stiffness (e.g., stiffening or softening spring) improves the MCK model, a post hoc analysis was attempted by adding a nonlinear spring term ($\alpha \cdot d(t)^3$) into the MCK model, which then becomes the Duffing equation representing a non-linear mass-spring-damper system [27]. The average R-sq utilizing the Duffing equation was 0.960 $\pm$ 0.051, which was worse than the MCK model (0.965 $\pm$ 0.049), further justifying the rejection of this model for future applications.

On the contrary, the PW model was generally able to mimic the experimental F-T responses without major issues (Fig. A2). Effective masses (M_2) determined from the PW model were very small (4.8 $\pm$ 6.1 grams), which implies that contribution of initial inertial responses, due to acceleration, to the F-T responses is negligible. Effective mass terms in the SLP was not used since acceleration returned to zero before the SLP began, as shown

in Figs. A1 and A2. The effective damping values determined from the ILP (5.6 $\pm$ 3.9 N-s/m) were smaller than those from the SLP (34.3 $\pm$ 28.4 N-s/m), while average effective stiffness for the ILP (3.0 $\pm$ 1.6 N/mm) was higher than that for the SLP (1.3 $\pm$ 1.0 N/mm) in the PW model. This implies that contribution of the force generated by the effective stiffness to the F-T response was higher in the ILP (e.g., linear elastic region) than the SLP, while contribution of the force induced by effective damping was higher in the SLP (e.g., non-linear plastic region) than the ILP. The rib displacement increased up to fracture, as shown in Fig. A1, so that the displacement data with the stiffness coefficients (e.g., spring force) was unable to replicate the flattened curves in the plastic region of the force. However, the velocity decreased after the elastic region of the force curve so that the velocity with damping coefficients (e.g., damping force) could replicate the flattened curves in the plastic region of the force data as shown in Fig. A1. The PW model was successfully able to characterize both linear and non-linear responses using spring and damping coefficients and kinematic data (i.e., acceleration, velocity and displacement) from the rib tests.

It should be noted that many previous studies assumed human ribs to be linear springs, in order to determine their structural stiffness [16-18]. The stiffness values published in [17] were directly compared to those determined from the PW model, particularly with K_{21} representing stiffness in linear regions in the ILP. Stiffness from the linear spring model (3.5 $\pm$ 1.8 N/mm) used in [17] was significantly higher than both K_{21} (3.0 $\pm$ 1.6 N/mm) and K_{22} (1.3 $\pm$ 1.0 N/mm) calculated from the PW model ($p<0.001$ for both K_{21} and K_{22}). This implies that the contribution of effective damping force to the rib F-T responses in the PW model cannot be ignored in the ILP, and it also explains why force induced from stiffness is smaller than that determined using a linear spring model. The PW model utilized entire time history curves, while the linear spring model used only the linear portion of F-D responses. In addition to this, defining the linear portions of the responses from structural tests, and even material tests, often requires subjective decision making [17][24-25]. However, the PW model does not introduce any subjectivity since it can objectively identify the linear and non-linear regions of F-T curves by determining the transition point in the optimization process (Eq.2).

To our knowledge, no previous studies have quantified structural viscous properties using whole ribs; therefore, direct comparison of the viscous properties to other studies is not possible. Lobdell et al. [20] developed an analytical model that replicated PMHS thoracic responses in frontal hub impacts [11-12]. They reported the effective damping coefficient for the thorax, including costal cartilage, sternum, ribs, thoracic viscera and other soft tissues, except the thoracic musculature, was 404.1 N-s/m after fitting the model to the PMHS thoracic force-deflection responses. In the PW model in our study, the average effective damping coefficient of ribs in the ILP was 5.6 N-s/m (1.4% of 404.1 N-s/m), while that in the SLP was 34.3 N-s/m (8.5% of 404.1 N-s/m). Based on this comparison, the contribution of the rib damping effect for a single rib into thoracic hub impact responses could possibly be less than 10%. Material elastic modulus of human bone has been used for enhancing scaling techniques for biomechanical responses of the thorax [23,26]. Thoracic responses in impact scenarios include more complicated behaviors than just simple linear elastic responses [11-12]. Based on Lobdell's analytical model [20] and the proposed PW model in this study, both thorax and ribs could be modeled using spring-damper connections. Therefore, both stiffness and damping coefficients can be used as important parameters that potentially improve current thoracic scaling techniques. With the large sample size of the ribs presented in this study, a new scaling approach using both stiffness and damping coefficients can be attempted in future work for various demographics (e.g., pediatric to elderly adult, sex and size specific).

Mimicking the plastic behavior of the pediatric ribs is a great benefit of the PW model. Exemplar plots for a pediatric rib (11 years) that shows both elastic and plastic responses and an old adult rib (82 years) that exhibits only elastic behavior are provided in Fig.B6 (a) and (b), respectively. It should be noted that the MCK model was not able to replicate the plastic behavior of the pediatric rib (R-sq = 0.919) but was able to replicate the elastic behavior of the old adult rib (R-sq = 0.999) as shown in Fig.A7. On the other hand, the PW model was able to characterize both elastic and plastic behavior of both ribs (R-sq > 0.995 for both pediatric and old adult ribs). The effective stiffness for both pediatric and adult ribs was larger in the ILP (K_{21}) than in the SLP (K_{22}), however, the pediatric ribs exhibited a larger reduction (from K_{21} of 1.5 N/mm to K_{22} of 0.2 N/mm) than the older adult ribs (from K_{21} of 1.1 N/mm to K_{22} of 0.8 N/mm). The damping coefficients, C_{21} and C_{22}, for the pediatric ribs (C_{21}: 7.0 N-s/m and C_{22}: 36.5 N-s/m) were greater than those for older adult ribs (C_{21}: 2.0 N-s/m and C_{22}: 3.8 N-s/m). The exemplar plots shown in Fig.A7 demonstrate how well the proposed PW model can capture the distinction between pediatric and older adult ribs. Since the PW model was capable of differentiating the stiffness and

damping coefficients between pediatric and adult ribs, these coefficients could potentially be used in future scaling techniques. Further investigation should be done to improve current scaling techniques using viscoelastic structural properties of the rib and thorax.

There are several limitations in this study. Ribs were tested only in the simplified frontal impact scenario. Hence, the results from this study should only be interpreted for the given testing scenario. Rib viscoelastic structural properties for side, oblique, and rear impacts should be investigated in the future. Unbalanced sample sizes between sexes could bias results, since more male data were used than female or pediatric. Further exploration should be done using more robust statistical methods, in order to investigate age, sex, and body size differences in conjunction with rib-, section-, and cortex-level predictors. The structural viscosity (i.e., damping coefficient) obtained in this study should not be deemed as the material viscosity. The structural viscoelastic properties presented in this study were dependent on the combination of structural effects and speed effects in the structural rib tests. Material viscoelastic properties should be determined in a separate study using a sophisticated material testing device with various input rates.

V. CONCLUSIONS

Viscoelastic structural properties of human ribs were investigated and presented in this study. The proposed piecewise model composed of M_2, C_{21}, C_{22}, K_{21}, and K_{22} allowed for successful replication of experimental elastic and plastic responses of human ribs. In general, effective stiffness largely contributed to the force responses for the ILP, while effective damping largely contributed to the force responses for the SLP. Due to the lack of viscoelastic structural properties of human ribs presented in the literature, these data should help researchers better understand rib structural characteristics in a simulated dynamic frontal impact scenario. These results can be applied to improve scaling techniques in the future.

VI. ACKNOWLEDGEMENT

First of all, we are very grateful to the anatomical tissue donors; their generous gifts made this research possible. Thanks to all of the students and staff of the Injury Biomechanics Research Center, USA, especially Arrianna Willis, Akshara Sreedhar, and Angela Harden. We are also grateful to Rod Herriott, Brian Suntay, and Colton Thomas from the Transportation Research Center, Inc., USA.

VII. REFERENCES

[1] Forman J, Poplin GS, et al. Automobile injury trends in the contemporary fleet: Belted occupants in frontal collisions. *Traffic Injury Prevention*, 2019, 20(6):607-612.

[2] Carroll J, Adolph T, et al. Overview of serious thorax injuries in European frontal car crash accidents and implications for crash test dummy development. *Proceedings of IRCOBI Conference*, Hannover, Germany 2010, IRC4-1: 217-234.

[3] Crandall J, Kent R, Patrie J, Fertile J, Martin P. Rib fracture patterns and radiologic detection–a restraint-based comparison. *Proceedings of Association for the Advancement of Automotive Medicine*, 2000, 44: 235-259.

[4] Kent R, Lee SH, et al. Structural and material changes in the aging thorax and their role in crash protection for older occupants. *Stapp Car Crash Journal*, 2005, 49: 231-249.

[5] Kent R, Woods W, Bostrom O. Fatality risk and the presence of rib fractures. *Proceedings of Advances in Automotive Medicine,* 2008, 52: 73-82.

[6] Pattimore D, Thomas P, Dave SH. Torso injury patterns and mechanisms in car crashes: an additional diagnostic tool. *Injury*, 1992, 23(2):123-126.

[7] Shimamura M, Ohhashi H, Yamazaki M. The effects of occupant age on patterns of rib fractures to belt-restrained drivers and front passengers in frontal crashes in Japan. *Stapp Car Crash Journal*, 2003, 47: 349-365.

[8] Shaw G, Lessley D, et al. Small female rib cage fracture in frontal sled tests. *Traffic Injury Prevention*. 2017, 18(1):77-82.

[9] Kang YS, Agnew AM, Hong CB, Icke K, Bolte JH. Elderly PMHS Thoracic Responses and Injuries in Frontal Impacts. *Proceedings of IRCOBI Conference*, Antwerp, Belgium, 2017, IRC-17-69: 539-557.
[10] Albert DL, Beeman SM, Kemper AR. Assessment of thoracic response and injury risk using the Hybrid III, THOR-M, and Post-Mortem Human Surrogates under various restraint conditions in full-scale frontal sled tests. *Stapp Car Crash Journal*, 2018, 62:1-65.
[11] Kroell CK, Schneider DC, Nahum AM. Impact tolerance and response of the human thorax. *Proceedings of 15th Stapp Car Crash Conference*, 1971, 710851.
[12] Kroell CK, Schneider DC, Nahum AM. Impact tolerance and response of the human thorax II. *Proceedings of 18th Stapp Car Crash Conference*, 1974, 741187.
[13] Shaw JM, Herriott RG, McFadden JD, Donnelly BR, Bolte JH. Oblique and lateral impact response of the PMHS thorax. *Stapp Car Crash Journal*, 2006, 50:147-167.
[14] Subit D, Salzar R. Ribcage kinematics under belt loading in intact, denuded and eviscerated conditions. *Proceedings of JSAE Congress*, 2014, 70-14:1-6.
[15] Kent R, Lessley D, Sherwood C. Thoracic response to dynamic, non-impact loading from a hub, distributed belt, diagonal belt, and double diagonal belts. *Stapp Car Crash Journal*, 2004, 48:495-519.
[16] Charpail E, Trosseille X, Petit P, Laporte S, Lavaste F, Vallancien G. Characterization of PMHS ribs: a new test methodology. *Stapp Car Crash Journal*, 2005, 49:183-198.
[17] Agnew AM, Murach MM, et al. Sources of Variability in Structural Bending Response of Pediatric and Adult Human Ribs in Dynamic Frontal Impacts. *Stapp Car Crash Journal*, 2018, 62:119-192.
[18] Kindig M, Lau AG, Kent RW. Biomechanical response of ribs under quasistatic frontal loading. *Traffic Injury Prevention*, 2011, 12(4):377-387.
[19] Daegling DJ, Warren MW, Hotzman JL, Self CJ. Structural analysis of human rib fracture and implications for forensic interpretation. *Journal of Forensic Sciences*, 2008, 53(6):1301-1307.
[20] Lobdell TE, Kroell CK, Schneider DC, Hering WE, Nahum AM. Impact response of the human thorax. In Human Impact Response, 1973:201-245. Springer, Boston, MA.
[21] Neathery R, Lobdell T. Mechanical simulation of human thorax under impact. *Proceedings of 18th Stapp Car Crash Conference*, 1973, 730982.
[22] Kent R, Bass CR, et al. Muscle tetanus and loading condition effects on the elastic and viscous characteristics of the thorax. *Traffic Injury Prevention*. 2003, 4(4):297-314.
[23] Mertz HJ, Irwin AL, Melvin JW, Stanaker RL, Beebe M. Size, weight and biomechanical impact response requirements for adult size small female and large male dummies. *SAE Technical Paper*, 1989, 890756.
[24] Kemper AR, McNally C, Pullins CA, Freeman LJ, Duma SM, Rouhana SW. The biomechanics of human ribs: material and structural properties from dynamic tension and bending tests. *Stapp Car Crash Journal*, 2007, 51:235-273.
[25] Albert DL, Kang YS, Agnew AM, Kemper AR. A comparison of rib structural and material properties from matched whole rib bending and tension coupon tests. *Proceedings of IRCOBI Conference*, 2017, Antwerp, Belgium, IRC-17-71: 567-576.
[26] Irwin AL, Mertz HJ. Biomechanical bases for the CRABI and Hybrid III child dummies. SAE Technical Paper, 1997, 973317.
[27] Kovacic I, Brennan MJ. The Duffing equation: nonlinear oscillators and their behaviour. John Wiley & Sons, Ltd. United Kingdom, 2011.

VIII. APPENDIX

Appendix A

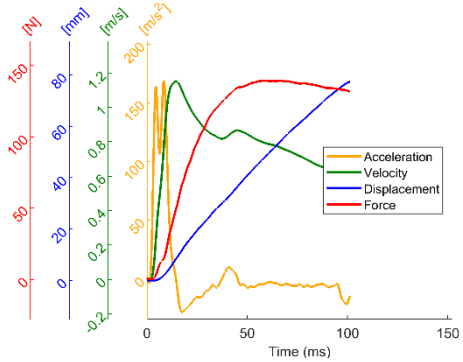

(a) Male 21 years

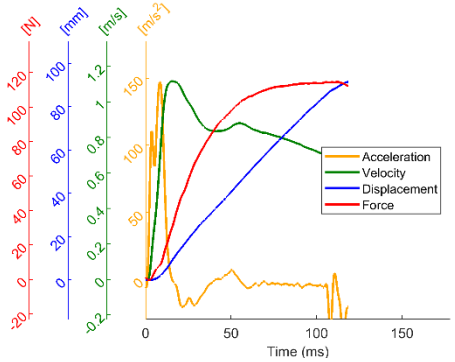

(b) Female 27 years

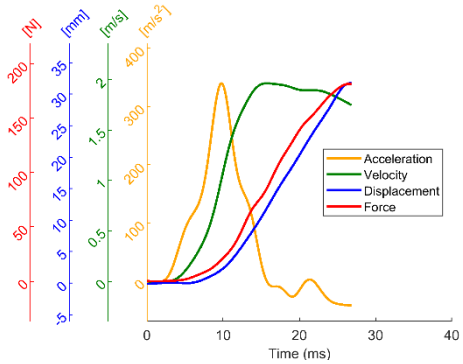

(c) Male 68 years

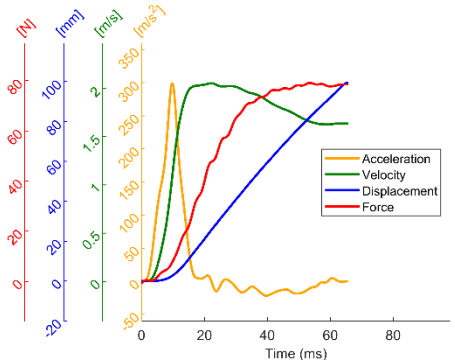

(d) Female 24 years

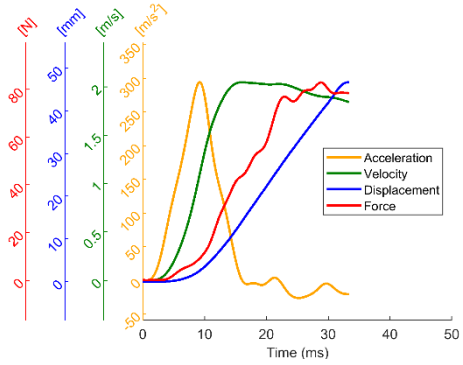

(e) Male 59 years

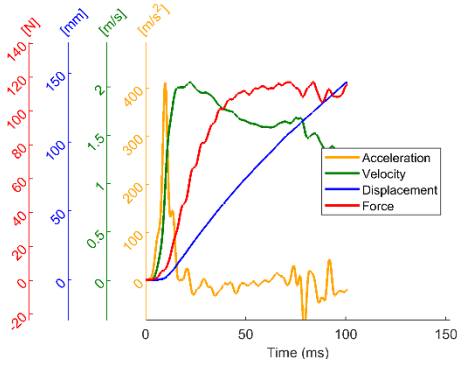

(f) Male 26 years

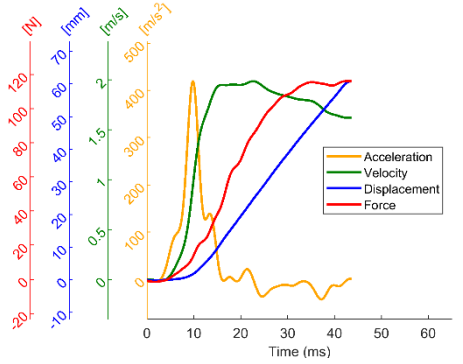

(g) Male 54 years

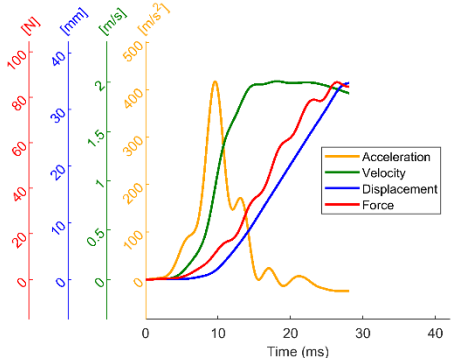

(h) Male 15 years

Fig. A1. Exemplar acceleration, velocity, displacement, and force time history plots.

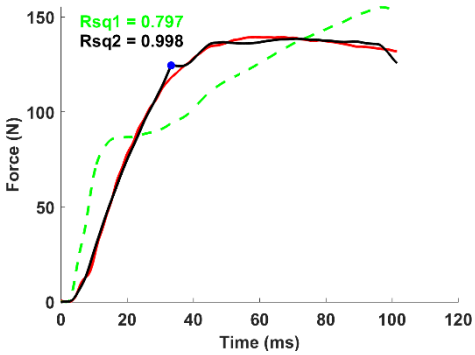

(a) Male 21 years

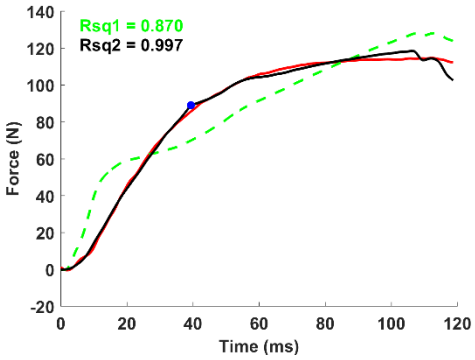

(b) Female 27 years

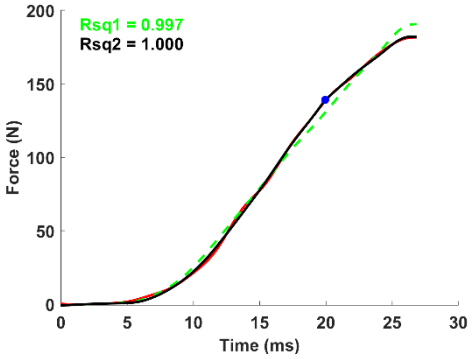

(c) Male 68 years

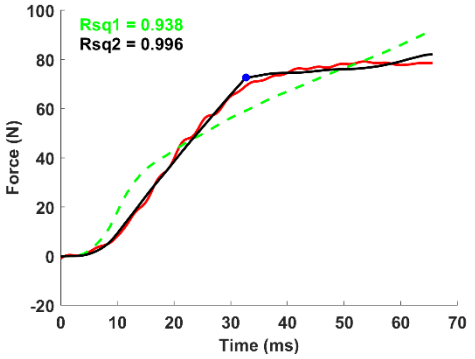

(d) Female 24 years

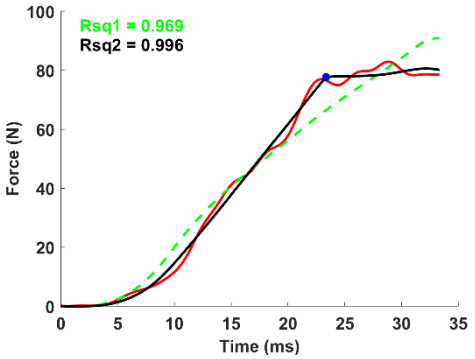

(e) Male 59 years

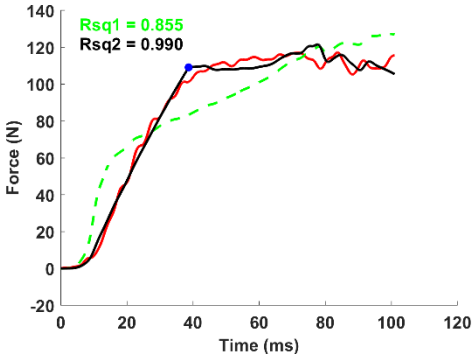

(f) Male 26 years

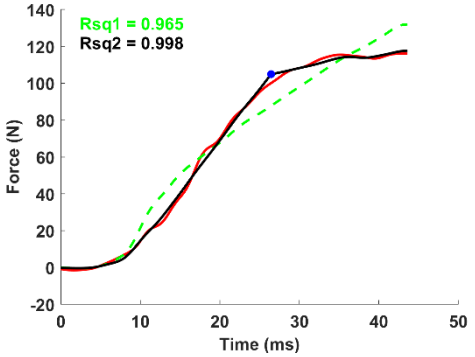

(g) Male 54 years

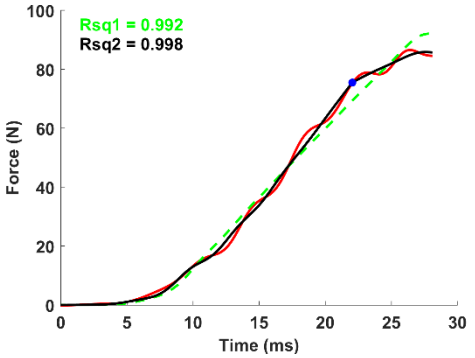

(h) Male 15 years

Fig. A2. Exemplar F-T plots showing experimental vs. analytical data. Red solid line: experimental data, green dash line: MCK model, black solid line: PW model. R-sq of 1.000 was due to rounding 0.9999.

Appendix B

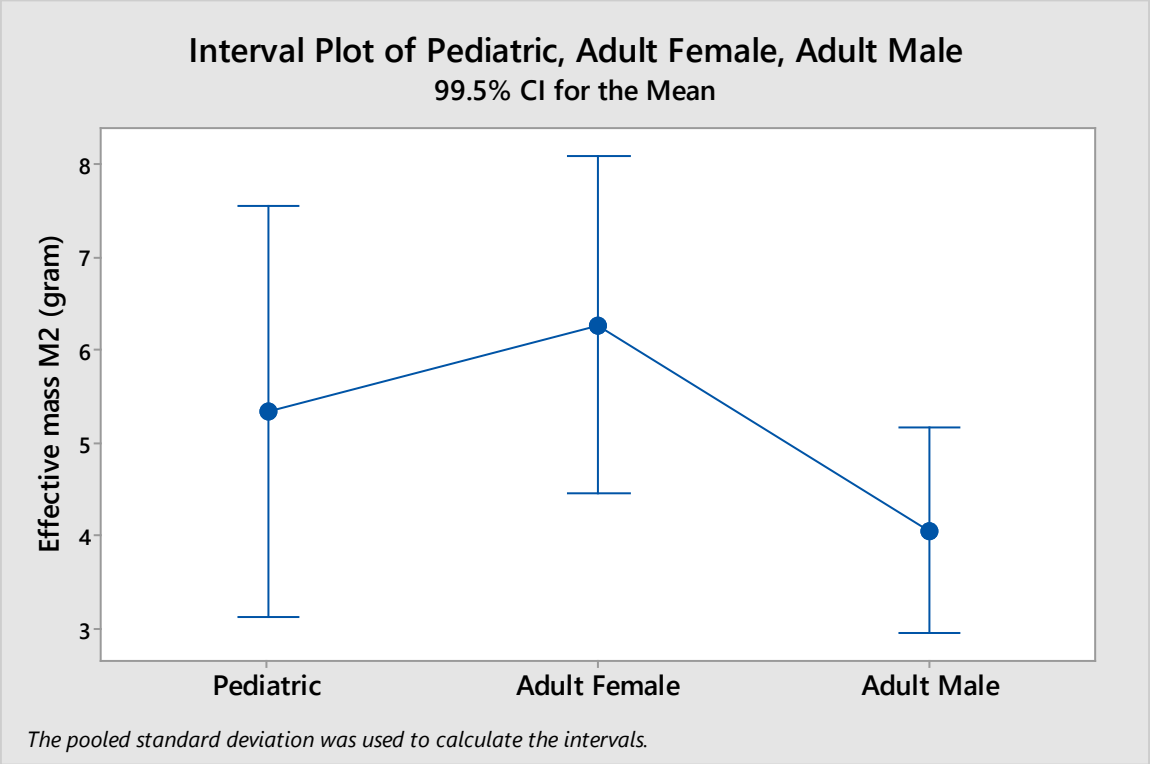

Fig. B1. Effective mass by group with 99.5% CI. No significant differences were found between groups (ANOVA, p = 0.01).

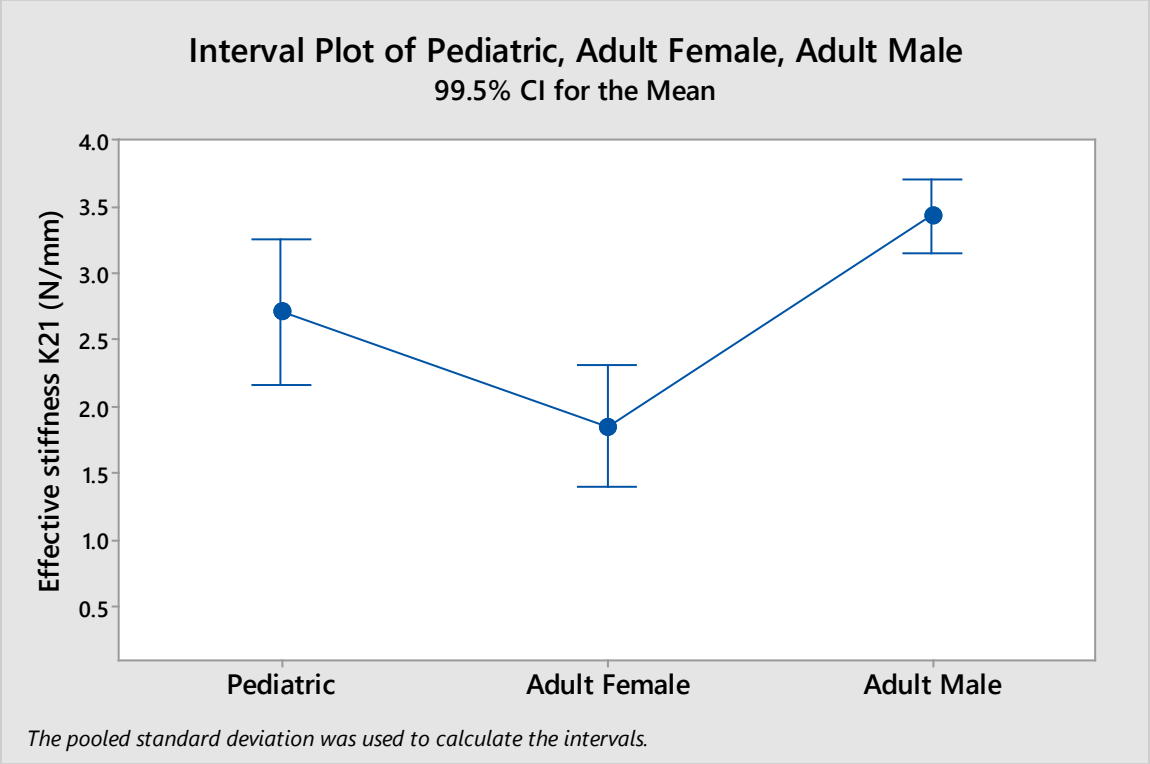

Fig. B2. Effective stiffness, K_{21}, by group with 99.5% CI. K_{21} varied significantly between groups, with adult male and pediatric ribs greater than adult females (ANOVA, p < 0.001).

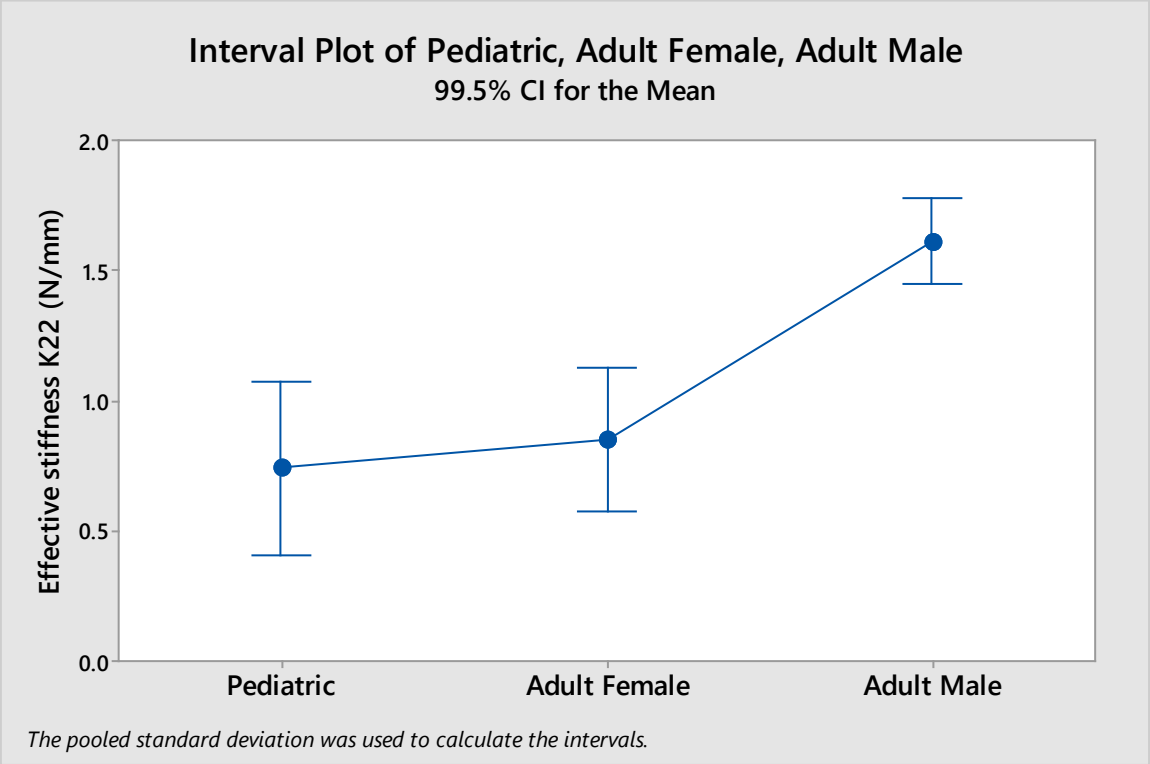

Fig. B3. Effective stiffness, K_{22}, by group with 99.5% CI. K_{22} varied significantly between groups, with pediatric and adult females significantly lower than adult males (ANOVA, $p < 0.001$).

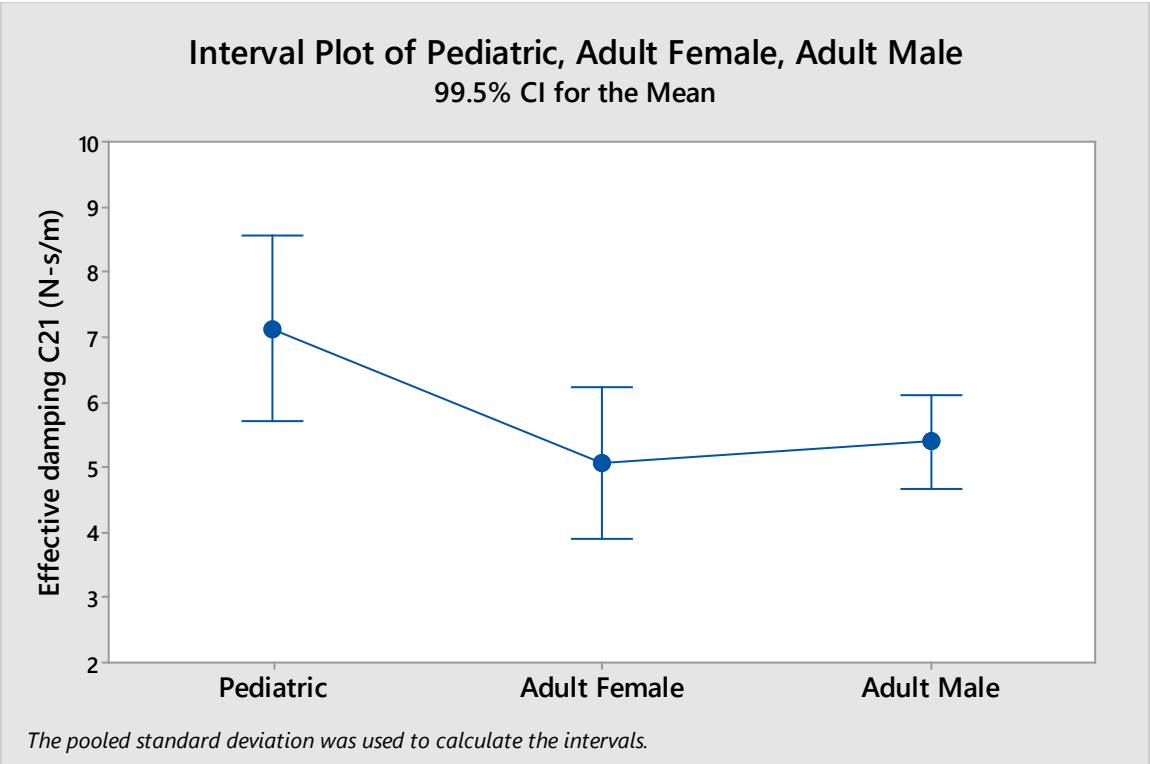

Fig. B4. Effective damping C_{21} by group with 99.5% CI. C_{21} varied significantly between groups, with the pediatric group having a greater mean than both other groups (ANOVA, $p = 0.003$).

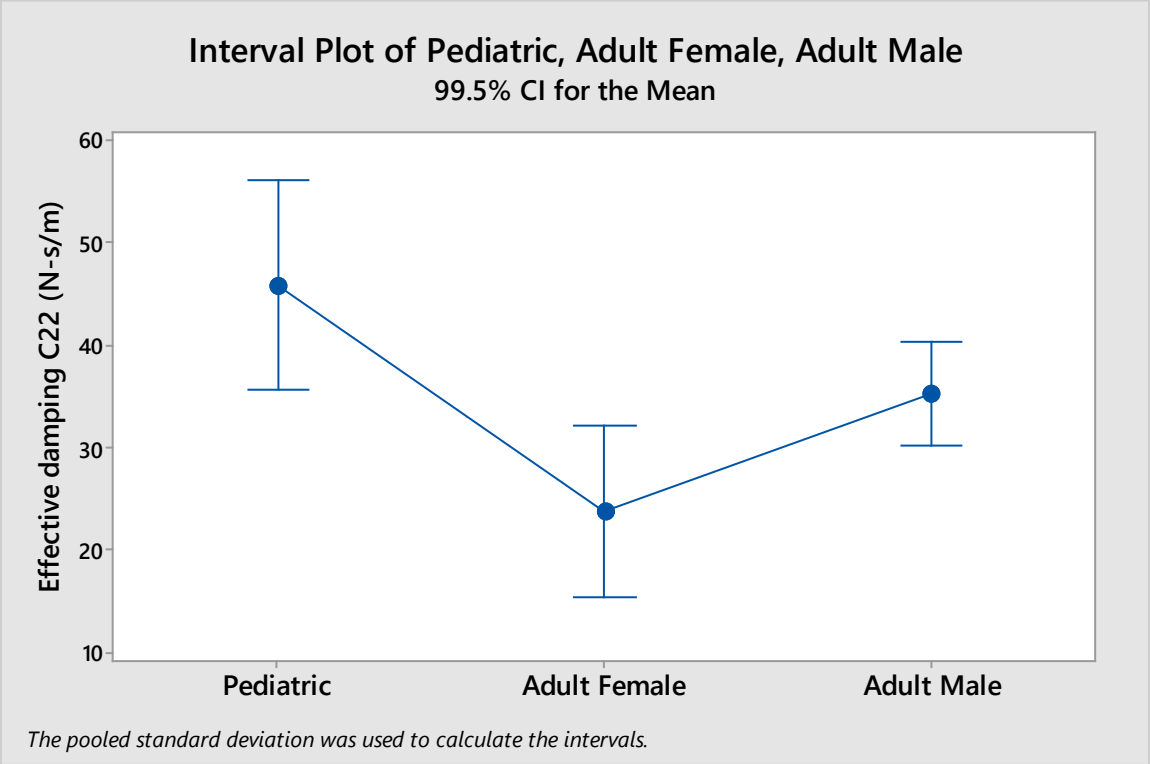

Fig. B5. Effective damping, C_{22}, by group with 99.5% CI. C_{22} varied significantly between groups, with the pediatric group having a greater mean than both other groups (ANOVA, $p < 0.001$).

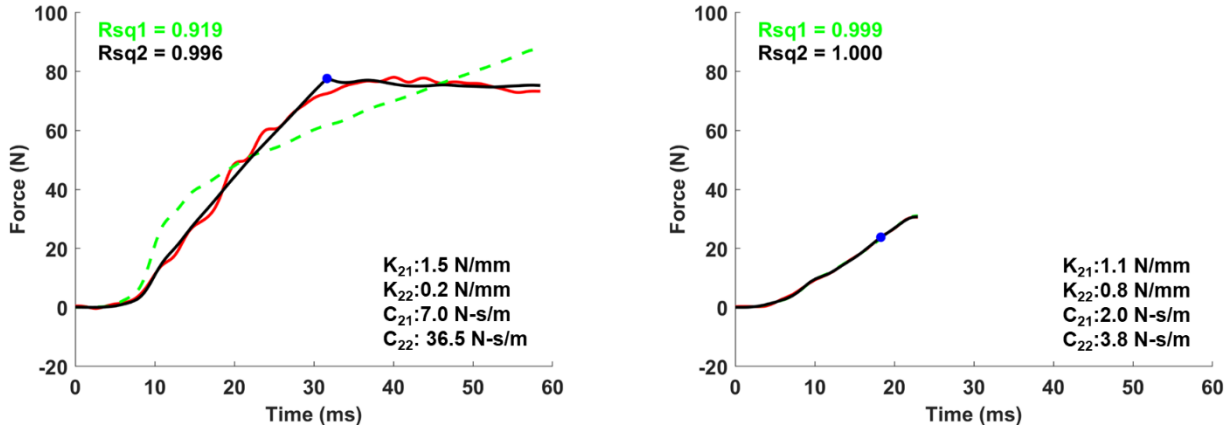

(a) Pediatric, 11 years (b) Female, 82 years

Fig. B6. Exemplar F-T plots for comparison of (a) pediatric rib to (b) old adult rib.